Measurement of the Proton Structure Function F_2 at Low Q^2

Andreas Meyer

DESY
Notkestr. 85, 22603 HAMBURG

Abstract. A measurement of the proton structure function $F_2(x, Q^2)$ is reported for momentum transfered squared Q^2 between 0.35 GeV^2 and 3.5 GeV^2 and for Bjorken-x values down to $6 \cdot 10^{-6}$. Towards low Q^2 the rise of F_2 with decreasing x is found to be less steep. The data are compared to different models. Presently, none of the models describes the data in the complete range which includes the photoproduction data at $Q^2 = 0$.

INTRODUCTION

The measurement extends the kinematic region w.r.t. former measurements [1–3] by a factor of 5 allowing to probe the transition between perturbative QCD (DIS) and Regge phenomenology (photoproduction). The extension was achieved by upgrading the H1 Detector in the backward region with a new drift chamber [4] and a lead/scintillating fibre calorimeter of spaghetti type (Spacal) [5]. The analysis is performed on 'shifted vertex data' recorded in 1995 where the ep interaction point was shifted by +70 cm along the proton direction extending the polar angular detector coverage to $\theta \leq 178.5°$. The results have been published recently in [6].

The cross section of the inclusive scattering process $ep \to eX$ is related to the proton structure function F_2 via

$$\frac{\mathrm{d}^2\sigma}{\mathrm{d}x\mathrm{d}Q^2} = \frac{2\pi\alpha}{Q^4 x}\left(2 - 2y + \frac{y^2}{1+R}\right) F_2(x, Q^2) \equiv \Gamma(y)\sigma^{\mathrm{eff}}_{\gamma^* p}(x, y, Q^2) \qquad (1)$$

where $R = F_L/(F_2 - F_L)$ and F_L is the longitudinal structure function. F_L has not yet directly been measured at HERA. For the extraction of F_2 from the measured cross section, an assumption on its value is made following a model [7]. The influence of F_L on the determination of F_2 from the measured cross section is neglegible at low values of the inelasticity y and less than 10%

everywhere. One can define $\sigma^{\text{eff}}_{\gamma^* p}$ as the effective measured virtual photon-proton cross section for ep collisions in the HERA kinematic range with the flux factor $\Gamma(y)$. Note that $\sigma^{\text{eff}}_{\gamma^* p}$ is independent from assumptions on F_L.

KINEMATIC RECONSTRUCTION

The measurement of both the scattered electron and the hadronic final state allows different ways of reconstructing the kinematic variables x and Q^2. In this analysis two methods are used, namely the "electron method" (E) using the angle and energy of the scattered electron only and the "Σ method" (Σ) [8] which uses both the hadronic final state and and the electron. E provides the best resolution at high values of y. Σ is most precise at low y and less sensitive to QED initial state radiation. The basic formulae for y are

$$y_e = 1 - \frac{E'_e}{E_e} \sin^2 \frac{\theta_e}{2}, \qquad y_\Sigma = \frac{\sum_{\text{hadrons}}(E - p_z)}{\sum(E - p_z)} \tag{2}$$

where E and E' are the energies of the incident and outgoing electron respectively and the polar scattering angle θ is calculated w.r.t. the direction of the proton beam. In both methods $Q^2 = p^2_{\perp,e}/(1-y)$ where $p_{\perp,e}$ is the transverse momentum of the scattered electron. The variable x is derived as $x = Q^2/ys$ where $\sqrt{s}$ is the ep center of mass Energy.

EVENT SELECTION

Events are selected by requiring an energy of more than 7 GeV of the most energetic cluster in the Spacal. Additional electron identification criteria, such as shower shape and track to cluster matching are imposed. A reconstructed vertex, necessary for the precise reconstruction of the event kinematics and the rejection of beam induced background, is required. Fig.1 shows the energy and angular distribution of electron candidates in the selected DIS event sample, together with Monte Carlo simulations (MC). For the simulation of the DIS events the DJANGO event generator [9] is used. The MC cross section is corrected by reweighting the MC events to the measured cross section. Background arises from small angle ep scattering ('photoproduction') where the scattered electron escapes undetected through the backward beam hole if at the same time the electron signature in the detector is 'faked' by hadronic final state particles. The photoproduction background is estimated using PHOJET [10]. Roughly 10% of the background events are tagged in the electron detector situated at -33m in the HERA tunnel. In Fig.2 the energy distribution of the tagged electrons (a) and the fake electrons (b) is shown together with the PHOJET simulation. The background is neglegible at low y and does not exceed 20% of the DIS signal anywhere. The ep cross section and F_2 are extracted subtracting the photoproduction background statistically.

RESULTS AND COMPARISONS TO MODELS

Fig.3(a) shows F_2 as a function of x in nine bins of Q^2 between 0.35 and 3.5 GeV^2. E and Σ methods are combined using E at high y, i.e. low x, thus optimizing the resolution. The data show that the rise of F_2 with decreasing x becomes smaller towards lower Q^2 values but is still prominent. Comparisons with previous results by H1 [1] and the fixed target exps. E665 [11] and NMC [12] show good agreement. Different parametrizations and models have been proposed to describe the region at low Q^2 and the transition from DIS to the photoproduction region. A recent review of the models can be found in [13]. The purely perturbative QCD (pQCD) prediction, represented by the GRV model [14], describes the data at values of $Q^2 > 1$ GeV^2. The DoLa model [15], based on Regge theory, represents the non-perturbative cross section. Although being significantly higher in all bins of Q^2 the data approach this prediction towards the lowest values of Q^2. The model by Badelek and Kwiecinski [16] (BK) uses a combination of a generalized Vector Meson Dominance Model (VMD) with dynamical parton models, which results in a smooth transition from the regime of pQCD to the lowest Q^2. It predicts the behaviour of the F_2 data very well. However, it fails to describe the photoproduction limit at $Q^2 = 0$. This is shown in Fig.3(b), plotting $\sigma^{\rm eff}_{\gamma^* p}$ as a function of Q^2 in different bins of W. The BK model overshoots the photoproduction data points [17] [18]. Also shown is a phenomenological parametrization achieved by reweighting the VMD and pQCD contributions used by BK in a fit including the photoproduction data.

SUMMARY

A measurement has been presented of the proton structure function $F_2(x, Q^2)$ in a range of 0.35 GeV^2 $< Q^2 <$3.5 GeV^2 exploring the transition region between pQCD and photoproduction. The data have been compared to different models. None of the models describes the data in the full range down to the photoproduction regime at $Q^2 = 0$. The dynamics in this region are still to be understood.

REFERENCES

1. H1 Collaboration, S. Aid et al., Nucl. Phys. **B470** (1996) 3.
2. ZEUS Collab., M. Derrick et al., Z. Phys. **C72** (1996) 399.
3. H1 Collaboration, C. Adloff et al., Phys. Lett. **B393** (1997) 452.
4. H1 Collab., DESY internal report PRC-93/02, (1993) 3006.
5. H1 Spacal Group, R.D. Appuhn et al.. DESY preprint 96-171, subm. to Nucl. Instr. Meth.
6. H1 Collaboration, **DESY-97-042**, subm. to Nucl. Phys. B, 1997.

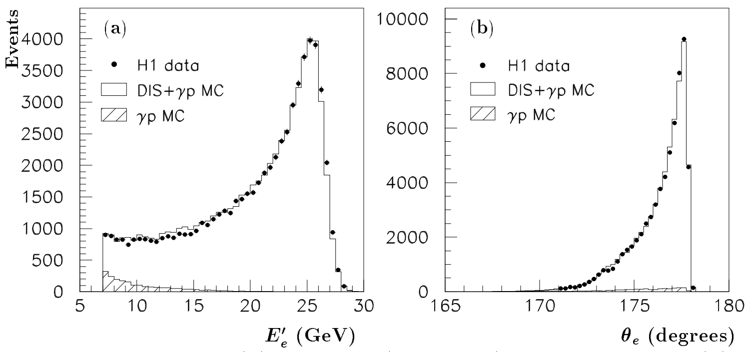

FIGURE 1. Experimental (•) and MC (solid line) distributions of (a) the energy and (b) the polar angle of the scattered electron for DIS events. The MC curves are the sum of DIS and photoproduction background. The hatched histogram depicts the photoproduction events alone.

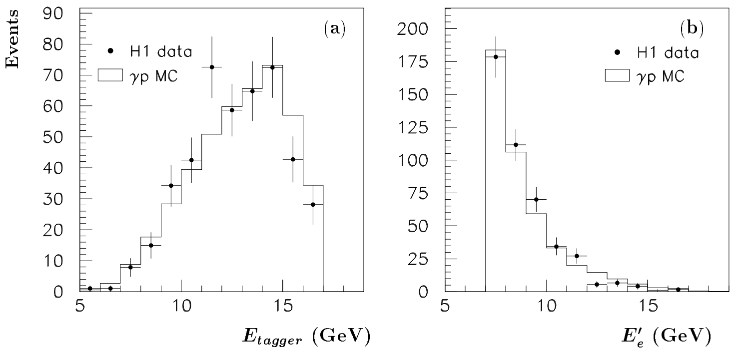

FIGURE 2. Experimental (•) and MC (solid line) distributions of (a) the energy of the scattered electron in the electron tagger and (b) the energy of the fake electron candidate in the Spacal, for tagged photoproduction events.

7. B. Badelek, J. Kwiecinski and A. Stasto, Durham **DTP/96/16**, 1996.
8. U. Bassler, G. Bernardi, Nucl. Instr. Meth. **A361** (1995) 231.
9. G.A. Schuler, H. Spiesberger, Proceedings of the Workshop Physics at HERA, vol. 3, Eds. W. Buchmüller and G. Ingelman, DESY (1992) 1419.
10. R. Engel and J. Ranft, Phys. Rev. **D54** (1996) 128.
11. E665 Collab., M.R. Adams et al., Phys. Rev. **D54** (1996) 3006.
12. NMC Collab., M. Arneodo et al., Phys. Lett. **B364** (1995) 107; NMC Collab., M. Arneodo et al., hep-ph/9610231 preprint, (1996).
13. A. Levy, DESY preprint DESY 97-013 (1997).
14. M. Glück, E. Reya and A. Vogt, Z. Phys. **C67** (1995) 433.
15. A. Donnachie and P. V. Landshoff, Z. Phys. **C61** (1994) 139.
16. B. Badelek, J. Kwiecinski, Phys. Lett. **B295** (1992) 263.
17. H1 Collab., T. Aid et al., Z. Phys. **C69** (1995) 27.
18. ZEUS Collab., M. Derrick et al., Z. Phys. **C63** (1994) 408.
19. A. Capella et al., Phys. Lett. **B337** (1994) 358.
20. K. Adel, F. Berreiro and F.J. Yndurain, FTUAM preprint 96-39 (1996).
21. H. Abramowitz, E.M. Levin, A. Levy, U. Maor, Phys. Lett. **B269** (1991) 465; Parametrization as presented in: A. Marcus Ph.D. thesis Tel-Aviv University TAUP 2350-96 (1996) (unpublished)

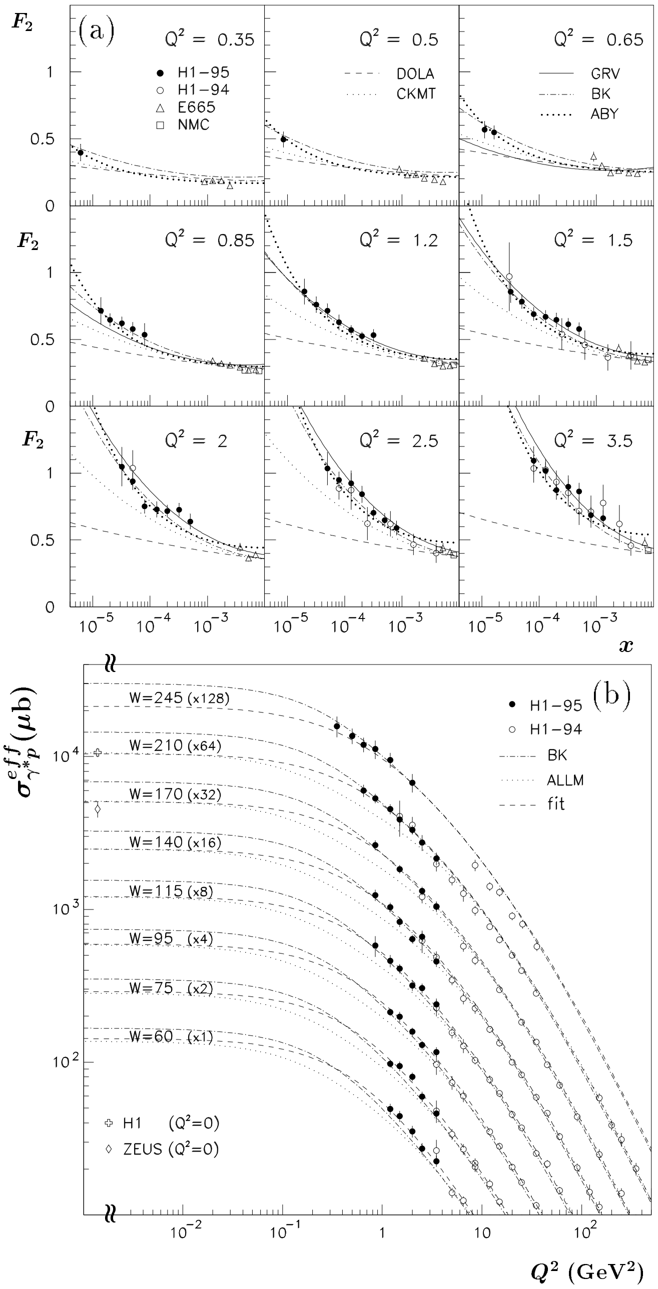

FIGURE 3. (a) Measurement of $F_2(x, Q^2)$ in nine bins of Q^2 by H1 (•). Also shown are previous results by H1(∘), E665(Δ) and NMC(□). The Q^2 values are given in GeV^2. Various models are shown: Donnachie and Landshoff (see text, dashed line), CKMT [19] (dotted line/small), BK (see text, dashed dotted line) GRV (full line) and ABY [20] (dotted line/large). (b) The virtual photon proton cross section $\sigma^{\rm eff}_{\gamma^* p}$ as a function of Q^2 for different bins of W. The photoproduction data refer to $Q^2 = 0$. The curves represent the ALLM [21] (dotted line) and BK parametrizations (dashed-dotted line) and the fit including the photoproduction data (solid line).